Modeling of Nanoelectronic and Quantum Devices*

D. K. Ferry, R. Akis, M. J. Gilbert, and G. Speyer

Department of Electrical Engineering and Center for Solid State Electronics Research
Arizona State University, Tempe, AZ 85287-5706

ABSTRACT

The semiconductor industry is constantly pushing towards ever smaller devices and it is expected that we will see commercial devices with gate lengths less than 10 nm within the next decade. Such small devices have active regions that are smaller than relevant coherence lengths, so that full quantum modeling will be required. In addition, novel new structures, such as molecules, may represent the active regions in such small devices. Here we outline a fully quantum mechanical approach to the modeling of coherent transport in ballistic structures. Examples of an SOI MOSFET and a molecule are presented.

Keywords: quantum transport, semiconductors, molecules, electron states, MOSFETs

1 INTRODUCTION

Almost 25 years ago, the prospects of making very small transistors was discussed, and a suggested technique for a 25 nm gate length, Schottky source-drain device, was proposed [1]. At that time, it was suggested that the central feature of transport in such small devices would be that the micro-dynamics could not be treated in isolation from the overall device environment (of a great many similar devices). Rather, it was thought that the transport would by necessity be described by quantum transport and that the array of such small devices on the chip would lead to considerable coherent many-device interactions. While this early suggestion does not seem to have been fulfilled, as witnessed by the quite normal behavior of today's research devices [2,3], there have been many subsequent suggestions for treatment via quantum transport [4-8]. There is ample suggestion that the transport will not be normal, but will have significant coherent transport effects and this, in turn, will lead to quantum behavior.

In this paper, we will review a full quantum formulation of the three dimensional transport, which is coupled to a three dimensional Poisson solver, in order to treat the coherent transport in small devices. In the next section, we will outline the basic approach, and then treat two example cases—a small silicon-on-insulator MOSFET, and a molecule attached to two conductors. Only the basic introduction to this approach is given, as more details are contained in the references and in a recent review article that is scheduled for publication [9].

* Work supported in part by the Office of Naval Research.

2 A QUANTUM TRANSPORT FORMULATION

There have been many suggestions for different quantum methods to model ultra-small semiconductor devices [10-12]. However, these approaches are uaually quasi-two-dimensional, as the length and the depth are modeled rigorously, while the third dimension (width) is usually included through the assumption that there is no interesting physics in this dimension. Other simulation proposals have simply assumed that only one sub-band in the orthogonal direction is occupied, therefore making higher-dimensional transport considerations unnecessary. These may not be valid assumptions, especially as we approach devices whose width is comparable to the channel length, both of which may be less than 10 nm.

It is important to consider all the modes that may be excited in the source (or drain) region, as this may be responsible for some of the interesting physics that we wish to capture. In the source, the modes are three dimensional (3D) in nature, even in a thin SOI device. These modes are propagated from the source to the channel, and the coupling among the various modes will be dependent upon the details of the total confining potential at each point along the channel. Moreover, as the doping and the Fermi level in short-channel MOSFETs increases, we can no longer assume that there is only one occupied sub-band. Hence, we use a full 3D quantum simulation, based on the use of recursive scattering matrices [13-16].

Consider the Schr dinger equation in three dimensions:

$$\frac{\hbar^2}{2}\frac{1}{m_x}\frac{d^2}{dx^2}\frac{1}{m_y}\frac{d^2}{dy^2}\frac{1}{m_z}\frac{d^2}{dz^2} \qquad . \qquad (1)$$

$$V(x,y,z) \qquad E$$

Here, it is assumed that the mass is constant, in order to simplify the equations (for nonparabolic bands, the reciprocal mass enters between the partial derivatives). We have labeled the mass corresponding to the principle coordinate axes. In silicon, these take on the values of m_L and m_T as appropriate. We then choose to implement this on a finite difference grid with uniform spacing a. Therefore, we replace the derivatives appearing in the discrete Schr dinger equation with finite difference representations of the derivatives. The Schr dinger equation then reads

$$
\begin{aligned}
& t_x\ \psi_{i\ \ 1,\ \ ,k} \quad \psi_{i\ \ 1,\ \ ,k} \\
& t_y\ \psi_{i,\ \ \ 1,k} \quad \psi_{i,\ \ \ 1,k} \\
& t_z\ \psi_{i,\ \ ,k\ \ 1} \quad \psi_{i,\ \ ,k\ \ 1} \\
& V_{i,\ \ ,k} \quad 2t_x \quad 2t_y \quad 2t_z\ \psi_{i,\ \ ,k} \\
& E\psi_{i,\ \ ,k} \quad ,
\end{aligned}
\tag{2}
$$

where t_x t_y and t_z are the hopping energies

$$
\begin{aligned}
t_x \quad & \frac{\hbar^2}{2m_x a^2}, \\
t_y \quad & \frac{\hbar^2}{2m_y a^2}, \\
t_z \quad & \frac{\hbar^2}{2m_z a^2}\ .
\end{aligned}
\tag{3}
$$

Each hopping energy corresponds with a specific direction in the silicon crystal. The fact that we are now dealing with three sets of hopping energies is quite important.

There are other important points that relate to the hopping energy. The discretization of the Schr dinger equation introduces an artificial band structure, due to the periodicity that this discretization introduces. As a result, the band structure in any one direction has a cosinusoidal variation with momentum eigenvalue (or mode index), and the total width of this band is 4t. Hence, if we are to properly simulate the real band behavior, which is quadratic in momentum, we need to keep the energies of interest below a value where the cosinusoidal variation deviates significantly from the parabolic behavior desired. For practical purposes, this means that $E_{\max}$ t. The smallest value of t corresponds to the longitudinal mass, and if we desire energies of the order of the source-drain bias ~ 1 V, then we must have a 0.2 nm. That is, we must take the grid size to be comparable to the Si lattice spacing

With the discrete form of the Schr dinger equation defined, we now seek to obtain the transfer matrices relating adjacent slices in our solution space. For this, we will develop the method in terms of slices [9]. This is modified here by the two dimensions in the transverse plane. We begin first by noting that the transverse plane has N_y N_z grid points. Normally, this would produce a second-rank tensor (matrix) for the wave function, and it would propagate via a fourth-rank tensor. However, we can re-order the coefficients into a N_yN_z 1 vector, so that the propagation is handled by a simpler matrix multiplication. Since the smaller dimension is the z direction, we use N_z for the expansion. Now, equation (2) can be rewritten as a matrix equation as, with s an index of the distance along the x direction,

$$
H\ (s)\ \ T_x\ \ (s\ \ 1)\ \ T_x\ \ (s\ \ 1)\ \ EI\ \ (s)\ . \tag{4}
$$

Here, I is the unit matrix, E is the energy to be found from the eigenvalue equation, and

$$
H \quad \begin{matrix}
H_0(\mathbf{r}) & \tilde{t}_z & \ldots & 0 \\
\tilde{t}_z & H_0(\mathbf{r}) & \ldots & \ldots \\
\ldots & \ldots & \ldots & \tilde{t}_z \\
0 & \ldots & \tilde{t}_z & H_0(\mathbf{r})
\end{matrix}\ , \tag{5}
$$

$$
T_x \quad \begin{matrix}
\tilde{t}_x & 0 & \ldots & 0 \\
0 & \tilde{t}_x & \ldots & 0 \\
\ldots & \ldots & \ldots & \ldots \\
0 & 0 & \ldots & \tilde{t}_x
\end{matrix}\ . \tag{6}
$$

The dimension of these two super-matrices is N_z N_z, while the basic Hamiltonian terms of (5) have dimension of N_y N_y, so that the total dimension of the above two matrices is N_yN_z N_yN_z. In general, if we take k and as indices along y, and η and ν as indices along z, then

$$
\tilde{t}_{z\ \ \eta\nu} \quad t_z\delta_{\eta\nu}\ ,\ \ \tilde{t}_{y\ \ k} \quad t_y\delta_k\ ,\ \ \tilde{t}_{x\ \ ss} \quad t_z\delta_{ss}\ , \tag{7}
$$

and

$$
H_0(\mathbf{r}) \quad \begin{matrix}
V(s,1,\eta) & W & t_y & \ldots & 0 \\
t_y & & V(s,2,\eta) & W & \ldots \\
\ldots & & \ldots & \ldots & t_y \\
0 & & 0 & t_y & V(s,N_y,\eta) \quad W
\end{matrix} \tag{8}
$$

The quantity W is $2(t_x \quad t_y \quad t_z)$.

With this set of matrices, the general procedure follows that laid out in the previous work. One first solves the eigenvalue problem on slice 0 at the end of the source (away from the channel), which determines the propagating and evanescent modes for a given Fermi energy in this region. The wave function is thus written in a mode basis, but this is immediately transformed to the site basis, and one propagates from the drain end, using the scattering matrice iteration

$$
\begin{matrix}
C_1(s\ \ 1) & C_2(s\ \ 1) \\
0 & 1
\end{matrix}
\quad
\begin{matrix}
0 & 1 \\
1 & (T_x)^{\ 1}\ EI\ \ H
\end{matrix}
\quad
\begin{matrix}
C_1(s) & C_2(s) & 1 & 0 \\
0 & 1 & P_1(s) & P_2(s)
\end{matrix} \tag{9}
$$

The dimension of these matrices is $2N_yN_z$ $2N_yN_z$, but the effective propagation is handled by submatrix compuations, through the fact that the second row of this equation sets the iteration conditions

$$
\begin{aligned}
& C_2(s\ \ 1) \quad P_2(s) \qquad C_2(s) \quad (T_x)^{\ 1}\ EI \quad H \quad^{1}, \\
& C_1(s\ \ 1) \quad P_1(s) \quad P_2(s)C_1(s).
\end{aligned}
\tag{10}
$$

At the source end, $C_1(0) = 1$, and $C_2(0) = 0$ are used as the initial conditions. These are now propagated to the N_x slice, which is the end of the active region, and then onto the $N_z + 1$ slice. At this point, the inverse of the mode-to-

site transformation matrix is applied to bring the solution back to the mode representation, so that the transmission coefficients of each mode can be computed. These are then summed to give the total transmission and this is used in a version of the Landauer formula to compute the current through the device (there is no integration over the transverse modes, only over the longitudinal density of states and energy).

3 AN SOI MOSFET

In the SOI MOSFET under consideration, we have an oversized source and drain region which are doped to 3 10^{19} cm^{-3} *n*-type. The dimensions of the source and the drain are 18 nm wide, 10 nm long and 6 nm high, corresponding to the thickness of the silicon (SOI) layer. The source and drain of the device have been given an exaggerated size to exacerbate the interaction of the modes excited in the source with the constriction present at the source-channel interface. The channel of our device is a *p*-type region. The channel is 10 nm in length, 6 nm in height and 8 nm in width. In the *z* direction of our device, the gate oxide has a thickness of 2 nm. Further, we have assumed that the oxide in this device is perfect in so much as the oxide does not have any spatial variation in thickness or charges present. Below the silicon layer, lies the buried oxide layer. This is 10 nm in thickness. This is large enough to insure that there is no leakage from the silicon layer, but also small enough to not waste computational resources simulating a region where no interesting physics is present. As discussed above, the *x* direction is along the channel, and the *z* direction is normal to the top gate. The simulation is carried out at low temperature. For this structure, we find that the threshold voltage is about 0.45 V, which does not vary much with doping in the channel, as there are only 2-3 dopants in the channel region. In Fig. 1, we illustrate the role of the impurities by plotting the local potential in the *x*-*y* plane, at the center of the channel. Here, both donors and acceptors are treated as discrete entities, and the potential clearly illustrates the local potential variations. The position of the dopant atoms has a significant effect on the resultant device characteristics. This is a result of the interference that the potential spikes produce. Dopants that are positioned closer to the source of the device have a greater effect on the threshold voltage than do dopants positioned further down the channel due to increased interaction with the waves incident at the source-channel interface, causing additional reflections.

In Fig. 2, we plot the density in a vertical cut through the *x*-*z* plane at the center of the channel, for a gate voltage of 1 V. Here, the source-drain bias is only 10 mV, but the conductance through the channel consists of one full mode propagating from the source to the drain [17]. However, looking at the figure, one does not draw this conclusion. Rather, the self-consistent potential has created quantum dots within the channel region, presumably due to quantum reflections at the source- and drain-interfaces with the channel, and it appears that the conductance is supported by resonant tunneling into and through this quantum dot. The actual position of the dot is bias dependent, and also depends upon the details of the location of the impurities in the channel.

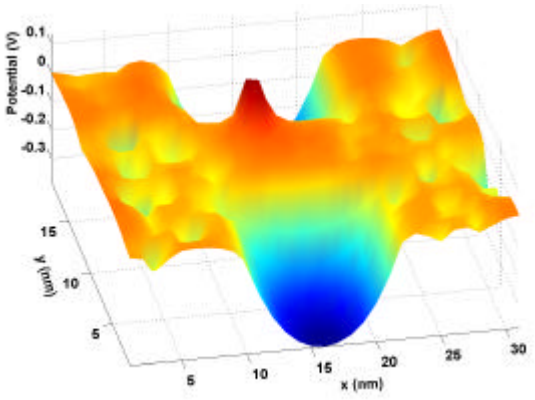

Fig. 1 The local potential in an x-y plane through the center of the channel. The gate voltage is 1 V, and the source-drain potential is 10 mV.

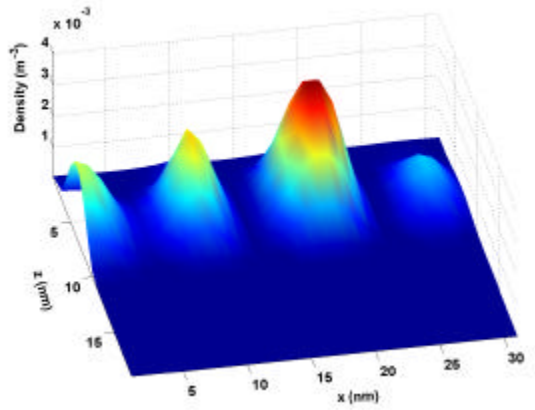

Fig. 2 density in a vertical (*x*-*z*) plane through the center of the channel. The gate is at the top, and the bottom region of no density is the SOI layer. Here, the gate bias is 1 V, and the source-drain bias is 10 mV.

The fact that the transport properties can be dramatically affected not only by the position in the *xy* plane, but by their position in the *z* direction as well, adds additional importance to such simulations. The positions of the dopants in the source and the drain can cause pools of electron density to form. This leads to noticeable variation in the density distribution in the source and, particularly, in the drain. This illustrates the growing importance of the mechanisms of coherence in ultra-short devices.

4 TRANSPORT IN A MOLECULE

As can be seen in eqn. (5), we need to know the Hamiltonian (energy spectrum) of the molecule in its configuration in order to use the recursive scattering matrix

approach. The first-principles program, FIREBALL 2000, a local atomic orbital density functional theory (DFT) based method in the local-density approximation (LDA), was used to calculate the Hamiltonian employed by the transfer matrix code [18]. We have first applied our approach to a xylyldithiol molecule connected to Au leads. Stretching of the molecule, corresponding to pulling the leads apart, has been simulated to compare with recent experiments [19]. In addition, FIREBALL 2000 was also used to calculate the Hellman-Feynman forces used to drift the xylyldithiol atoms upon stretching. In order to preserve the periodicity of the unit cell, the gold atoms were left fixed in these simulations, although the dynamics of the gold atoms are believed to be important in the stretching. Molecules were initially attached in the hollow-site configuration.

Our calculations agree within an order of magnitude with experimental calculations of the molecular conductance and indicate an interesting trend in the conductance upon stretching, with an apparent resonance for ~0.2 nm. Orbital plots [20] help explain this phenomenon. As the molecule is stretched, orbitals near the Fermi level change in degree of localization. At the resonance, there is a conductance enhancement due to the planarization of the molecule leading to enhanced coupling between gold states and molecular states. This is evident in the LUMO-like orbital, as shown in Fig. 3. We also note the effect of charge transfer at the metal-molecule interface with applied bias, agreeing well with other theoretical observations [21].

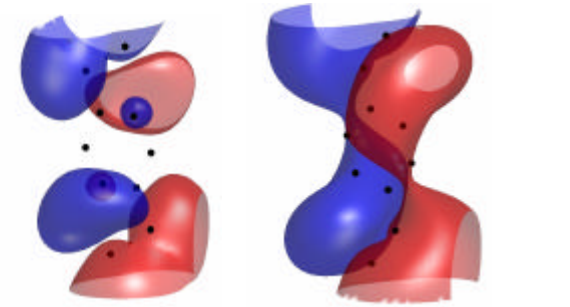

Fig. 3 Difference in the LUMO level at 0.06 nm (left) and 0.2 nm (right) stretch of the xylyldithiol molecule. The dots are atomic positions.

5 CONCLUSIONS

Coherent transport is becoming much more important in real semiconductor devices as the gate length is reduced into the nanometer regime. Hence, the role of coherent effects in device operation become important, and the control of decoherence within the source and drain assumes more importance [22]. We have developed a series of fully three dimensional quantum transport models, coupled with three dimensional Poisson solvers, to investigate such coherent transport in small systems. This has been illustrated here with an SOI MOSFET, and a molecule attached to two gold leads. These approaches are quite general and provide an alternative approach to other methods which have recently appeared in the literature [10-12, 23].

REFERENCES

[1] J. R. Barker and D. K. Ferry, Sol.-State Electron 23, 531, 1980.

[2] R. Chau, 2001 Silicon Nanoelectronics Workshop, Kyoto, Japan, June 10-11, 2001.

[3] B. Doris, M. Ieong, T. Kanarsky, Y. Zhang, R. A. Roy, O. Dokumaci, Z. Ren, F.-F. Jamin, L. Shi, W. Natzle, H.-J. Huang, J. Mezzapelle, A. Mocuta, S. Womack, M. Gribelyuk, E. C. Jones, R. J. Miller, H.-S. P. Wong, and W. Haensch, 2002 International Electron Device Meeting Technical Digest. New York: IEEE, 2002:267-270.

[4] M. Fischetti, J Appl Phys. 83, 270, 1998.

[5] K. Likharev, In: Morko H, ed. Advanced Semiconductor and Organic Nano-Technique. New York: Academic, 2002.

[6] R. Venugopal, Z. Ren, S. Datta, M. S. Lundstrom, and D. Jovanovic, J. Appl. Phys. 92, 3730, 2002.

[7] K. Natori, J. Appl. Phys. 76, 4879, 1994.

[8] M. J. Gilbert, R. Akis, and D. K. Ferry, J. Comp. Electron. *In press*.

[9] D. K. Ferry, R. Akis, M. J. Gilbert, and S. M. Ramey, to be published in *Silicon Nanoelectroncs*, S. Oda and D. K. Ferry, Eds., *in preparation*.

[10] F. G. Pikus, and K. K. Likharev, Appl. Phys. Lett.; 71, 3661, 1997.

[11] S. Datta, Superlatt Microstuct. 28, 253, 2000.

[12] J. Knoch, B. Lengeler, and J. Appenzeller, IEEE Trans. Elec. Dev. 49, 1212, 2002.

[13] T. Usuki, M. Takatsu, R. A. Kiehl, and N. Yokoyama, Phys. Rev. B, 50, 7615, 1994.

[14] T. Usuki, M. Saito, M. Takatsu, R. A. Kiehl, and N. Yokoyama, Phys. Rev. B, 52, 8244, 1995.

[15] R. Akis, D.K. Ferry, and J. P. Bird, Phys. Rev. B, 54, 17705, 1996.

[16] M. J. Gilbert, S. N. Milicic, R. Akis, and D. K. Ferry, IEEE Trans. Nanotechnolog., *In press*.

[17] M. J. Gilbert and D. K. Ferry, Superlatt. Microstruc., *in press*.

[18] O. F. Sankey and D. J. Niklewski, Phys.Rev. B 40, 3979, 1989.

[19] B. Xu and N. J. Tao, Science 301, 1221, 2003.

[20] G. Speyer, R. Akis, and D. K. Ferry, Superlatt. Microstruc., *in press*.

[21] Y. Xue and M. A. Ratner, Phys Rev. B 68, 115406, 2003.

[22] D. K. Ferry and J. R. Barker, Appl. Phys. Lett. 74, 582, 1999.

[23] M. Brandbyge, J.-L. Mozos, P. Ordejon, J. Taylor, and K. Stokbro, Phys. Rev. B 65, 165401, 2002.